Algorithms & Systems for Optical Information Processing IV

Vol. 4113

PROCEEDINGS OF SPIE
SPIE—The International Society for Optical Engineering

Algorithms and Systems for Optical Information Processing IV

Bahram Javidi
Demetri Psaltis
Chairs/Editors

1–2 August 2000
San Diego, USA

Sponsored and Published by
SPIE—The International Society for Optical Engineering

Volume 4113

SPIE is an international technical society dedicated to advancing engineering and scientific applications of optical, photonic, imaging, electronic, and optoelectronic technologies.

Please use the following format to cite material from this book:

Author(s), "Title of paper," in *Algorithms and Systems for Optical Information Processing IV*, Bahram Javidi, Demetri Psaltis, Editors, Proceedings of SPIE Vol. 4113, page numbers (2000).

ISSN 0277-786X
ISBN 0-8194-3758-1

Published by
SPIE—The International Society for Optical Engineering
P.O. Box 10, Bellingham, Washington 98227-0010 USA
Telephone 1 360/676-3290 (Pacific Time) • Fax 1 360/647-1445
http://www.spie.org/

Printed in the United States of America.

Contents

vii *Conference Committee*

KEYNOTE PAPER

1 **Nonlinear space-time information processing** [4113-01]
P. C. Sun, D. M. Marom, D. Panasenko, R. I. Rokitski, P. C. Lin, K. Oba, Y. T. Mazurenko, Y. Fainman, Univ. of California/San Diego (USA)

SESSION 1 IMAGE RECOGNITION I

13 **Chromatically compensated multichannel optical correlators (Invited Paper)** [4113-02]
P. B. Andrés, Univ. de Valencia (Spain); V. Climent, Univ. Jaume I (Spain)

23 **Optical-correlator-based system for the real-time analysis of image motion in the focal plane of an Earth observation camera** [4113-03]
V. Tchernykh, S. V. Dyblenko, K. Janschek, Dresden Univ. of Technology (Germany); B. Harnisch, European Space Agency/ESTEC (Netherlands)

32 **Image processing for new optical pattern recognition encoders** [4113-04]
D. B. Leviton, NASA Goddard Space Flight Ctr. (USA)

SESSION 2 IMAGE RECOGNITION II

41 **Computer simulation results for a Hilbert transform optical correlator** [4113-05]
A. D. McAulay, Lehigh Univ. (USA)

49 **High-speed correlation employing chirp-encoded binary phase-only patterns** [4113-06]
B. S. Lowans, M. F. Lewis, C. V. Peck, Defence Evaluation and Research Agency Malvern (UK)

59 **Feature extraction by use of an array of the Hough transform filters** [4113-07]
J.-S. Jang, D.-H. Shin, Pukyong National Univ. (Korea)

68 **Power cepstral image analysis through the scale transform** [4113-08]
J. L. Pech-Pacheco, G. Cristóbal, Instituto de Optica (Spain); J. Alvarez-Borrego, CICESE\Física Aplicada (Mexico); L. Cohen, CUNY/Hunter College and Graduate Ctr. (USA)

80 **Nonlinear correlation with Gaussian filter in the Fourier domain** [4113-29]
S. Kishk, S. Verrall, B. Javidi, Univ. of Connecticut (USA)

SESSION 3 IMAGE PROCESSING I

86 **Surface and defect analysis using spatial light modulators (Invited Paper)** [4113-09]
H. J. Tiziani, T. Haist, Univ. Stuttgart (Germany)

96 **Optical signal processing using spatiotemporal dynamic system with spatial light modulator (Invited Paper)** [4113-10]
Y. Hayasaki, H. Yamamoto, N. Nishida, Univ. of Tokushima (Japan)

106 **Segmenting shadows from synthetic aperture radar imagery using edge-enhanced region growing** [4113-11]
G. J. Power, K. S. Wilson, Air Force Research Lab. (USA)

115 **Optical classification of random image fields using spectral synthetic discriminant functions** [4113-12]
A. S. Ostrovsky, E. Pino Mota, J. I. Palma Cuatianquiz, Univ. Autónoma de Puebla (Mexico)

SESSION 4 IMAGE PROCESSING II

123 **Development of a multispectral autoradiography using a coded aperture** [4113-13]
D. Noto, Yamagata Univ. (Japan); T. Takeda, J. Wu, T. T. Lwin, Univ. of Tsukuba (Japan); Q. Yu, T. Zeniya, T. Yuasa, Y. Hiranaka, Yamagata Univ. (Japan); Y. Itai, Univ. of Tsukuba (Japan); T. Akatuka, Yamagata Univ. (Japan)

134 **Analysis of decision boundaries of radial basis function neural networks** [4113-14]
E. Jung, C. Lee, Yonsei Univ. (Korea)

143 **New modified fuzzy C-means algorithm for synthetic aperture radar (SAR) image segmentation** [4113-15]
P. Thitimajshima, King Mongkut's Institute of Technology Ladkrabang (Thailand)

148 **Fast CGH algorithm for the off-plane near-field computer-generated hologram** [4113-16]
K. Kim, J. Chun, Korea Advanced Institute of Science and Technology; J. Sohn, J. Cho, Korea Institute of Science and Technology

SESSION 5 OPTICAL SECURITY I

156 **Programmable optical security systems using computer-generated holography (Invited Paper)** [4113-18]
T. Nomura, Wakayama Univ. (Japan); B. Javidi, Univ. of Connecticut (USA)

165 **Random encoded reference beam for secure data storage in a holographic memory** [4113-19]
V. B. Markov, D. C. Weber, MetroLaser, Inc. (USA)

176 **Recognition of occluded images by dual nonlinear correlation** [4113-20]
K. Chałasińska-Macukow, R. Wasążnik, Warsaw Univ. (Poland)

181 **Improvement of the signal-to-noise ratio of a double random phase encoding encryption system** [4113-21]
W.-C. Su, B. Wang, C.-C. Sun, National Central Univ. (Taiwan); M.-W. Chang, Yuan-Ze Univ. (Taiwan)

SESSION 6 OPTICAL SECURITY II

187 **Influence of information content of partially occluded images on the results of recognition** [4113-22]
K. Chałasińska-Macukow, M. Rowicki, W. Stachera, Z. Chról, R. Kotyński, Warsaw Univ. (Poland)

194 **Comparative analysis of optical and hybrid joint transform correlators for security applications** [4113-23]
L. I. Muravsky, Y. P. Kulynych, O. P. Maksymenko, T. I. Voronyak, I. Y. Pogan, Institute of Physics and Mechanics (Ukraine); F. L. Vladimirov, S.I. Vavilov State Optical Institute (Russia); S. A. Kostyukevych, Institute of Semiconductor Physics (Ukraine)

205 **Heuristic algorithm for calculation of sufficiently randomized object-independent diffuser for holography** [4113-24]
B. B. Chhetri, S. Serikawa, T. Shimomura, Kyushu Institute of Technology (Japan)

217 **Analyzing decision boundaries of neural networks** [4113-28]
C. Lee, E. Jung, Yonsei Univ. (Korea)

227 **Computer-generated digital holograms based on IFS and application** [4113-25]
H. Cao, G. Zhu, Y. Zhu, Z. Zhang, H. Ge, X. Li, Huazhong Univ. of Science and Technology (China)

POSTER SESSION

234 **Error dispersion algorithms to improve the precision of angle detection for the optical encoder** [4113-26]
Y. Matsuzoe, N. Tsuji, Fuji Electric Co., Ltd. (Japan); T. Yoshizawa, Tokyo Univ. of Agriculture and Technology (Japan)

242 **Quantitative evaluation of visual performance of liquid crystal displays** [4113-27]
Y. Mori, K. Tanahashi, S. Tsuji, IBM Japan, Ltd.

251 *Addendum*
252 *Author Index*

Conference Committee

Conference Chairs

Bahram Javidi, University of Connecticut (USA)
Demetri Psaltis, California Institute of Technology (USA)

Program Committee

Henri H. Arsenault, COPL/University Laval (Canada)
George Barbastathis, Massachusetts Institute of Technology (USA)
David P. Casasent, Carnegie Mellon University (USA)
H. John Caulfield, Diversified Research Corporation (USA)
Pierre H. Chavel, Institut d'Optique (France)
Charles G. Garvin, Sanders, A Lockheed Martin Company (USA)
Joseph L. Horner, Air Force Research Laboratory (USA)
James C. Kirsch, U.S. Army Aviation and Missile Command
Ahmed Louri, University of Arizona (USA)
Abhijit Mahalanobis, Raytheon Missile Systems Company (USA)
Emanuel Marom, Tel Aviv University (Israel)
Alastair D. McAulay, Lehigh University (USA)
David Mendelovic, Tel Aviv University (Israel)
Nasser M. Nasrabadi, Army Research Laboratory (USA)
Philippe Réfrégier, École Nationale Supérieure de Physique de Marseille (France)
Nabeel A. Riza, CREOL/University of Central Florida (USA)
Edmund G. Zelnio, Air Force Research Laboratory (USA)

Session Chairs

Image Recognition I
Takanori Nomura, Wakayama University (Japan)

Image Recognition II
Alastair D. McAulay, Lehigh University (USA)

Image Processing I
Hans J. Tiziani, Universität Stuttgart (Germany)

Image Processing II
Pedro B. Andrés, Universidad de Valencia (Spain)

Optical Security I
Thomas R. Lettieri, National Institute of Standards and Technology (USA)

Optical Security II
Katarzyna Chałasińska-Macukow, Warsaw University (Poland)

Keynote Paper

Nonlinear Space-Time Information Processing

P. C. Sun*, D. M. Marom, D. Panasenko, R. I. Rokitski, P. C. Lin, K. Oba

Y. T. Mazurenko, Y. Fainman

Department of Electrical and Computer Engineering, Univ. of California/San Diego

ABSTRACT

Nonlinear optical processing techniques that produce space-time information processing are introduced and experimentally demonstrated. The basic concept of such space-time processors closely resembles conventional Fourier optical processors of the space domain. By using ultrafast short pulses and nonlinear optics, we can perform not only real-time optical information conversion between the space and time domains, but also the processing and imaging of temporal information.

KEY WORDS: nonlinear information processing, four-wave mixing, pulse imaging, space-time process

1. INTRODUCTION

Ultrashort pulse laser technology has recently experienced significant advances, producing high peak power pulses of optical radiation a few femtoseconds in duration, corresponding to only a few cycles of its fundamental frequency. Future progress in this area is inevitable due to unique properties of ultrashort laser pulses that are crucial for various science and engineering applications including optical communications, medical and biomedical imaging, chemistry and physics. In communication applications, pulse laser technology enables the bandwidth and the efficiency of fiber optic communications systems to exceed those of electrical cable systems. To implement these applications, it will be necessary to construct an all-optical pre-processor at the transmitter and a post-processor at the receiver, which will perform multiplexing, and demultiplexing, respectively. The multiplexer performing space-to-time transformation will combine relatively slow but parallel electronic channels into an ultrahigh bandwidth serial fiber optic channel (i.e., parallel-to-serial conversion), whereas the demultiplexer will perform the inverse time-to-space transformation for electronic detection (i.e., serial-to-parallel conversion). Parallel-to-serial format conversion I/O devices will need to be developed for integration of such page oriented storage systems with communication network systems. In order to meet the speed requirement of the ultrahigh bandwidth of fiber communication networks, such data transformation between the space and time domain need to be operated in real-time, i.e. in a speed of femtosecond rate. Therefore, a nonlinear optical approach becomes unavoidable for these applications.

We use the term "nonlinear information processing" to show that many of these nonlinear processing techniques closely resemble traditional linear optical information processing techniques, such as those learned from Fourier optics. The emphasis of Fourier optics was applied to optical information in the space domain. Now, with the help of nonlinear optics and ultrafast pulse lasers, we can extend the whole concept into the time domain which allows processing of optical information with temporal distribution. In addition, optical information now can be converted between the space and time domain via nonlinear information processing. In this paper, we will provide an overview of the nonlinear information processing techniques that have been demonstrated by our group and others in recent years. We distinguish between different applications by placing emphasis on two major groups: (1) Nonlinear space-time processing, and (2) Temporal information processing.

2. NONLINEAR SPACE-TIME PROCESSING

2.1 Space-To-Time Conversion Processors (STCP)

2.1.1 Pulse Shaper

A straightforward technique to implement STCP uses a spectral domain pulse shaper. This device is based on spectral decomposition of an ultrashort transform-limited laser pulse into the spectral domain,

*Correspondence: E-mail:pcaun@ece.ucsd.edu; WWW: http://kfir.ucsd.edu/Members/sun.shtml; tel:858-534-7891

Algorithms and Systems for Optical Information Processing IV, Bahram Javidi, Demetri Psaltis, Editors, Proceedings of SPIE Vol. 4113 (2000) © 2000 SPIE. · 0277-786X/00/$15.00

modifying the pulse spectrum by using a 1D fixed[1] or programmable [2,3] spatial mask and recombining the modified temporal spectrum back into the time domain to form a shaped pulse. This technique has been shown to produce femtosecond shaped pulse trains with terahertz repetition rate, high resolution, and high fidelity.[4] For communication applications, the pulse shaping device needs to be operated in real time, which will require not only fast computation, but also fast I/O bandwidth spatial light modulators (SLM) that can meet the spatial resolution and the dynamic range of such spatial Fourier transform devices. The liquid crystal SLMs[2] and the acousto-optic SLMs[3] that are currently being used for such a dynamic pulse shaping have limited speed, resolution, and dynamic range, limiting their potential use for ultra-high bandwidth optical communication applications.

2.1.2 Photorefractive Four-wave Mixing

We have addressed some of these difficulties by introducing an all-optical parallel-to-serial processor that is capable of converting directly spatial optical signals into temporal shaped pulses with a one-to-one correspondence[5]. Our approach is based on combining an optical information processing technique that uses spectral holography [6,7] with that of conventional spatial Fourier transform holography. Our processor, shown schematically in Fig. 1a, consists of two independent optical channels for carrying the temporal and the spatial information. The temporal information-carrying channel consists of a pair of gratings and a 4-F lens arrangement. The spatial information-carrying channel is a simple optical spatial Fourier transform arrangement consisting of the input image plane and a beamsplitter to share the second lens of the temporal channel. To achieve interaction between the temporal and spatial frequency spectral information we use a real time holographic material in a degenerate four-wave mixing arrangement.

For our initial experiment we used a 1-D binary input image (or a 1-D spatial light modulator) illuminated by a monochromatic optical source and Fourier transformed into the plane of the real-time holographic material where it interferes with the plane reference wave. The interference pattern via the photorefractive effect causes recording of a spatial Fourier transform hologram. The recorded spatial Fourier transform hologram is reconstructed by the temporal frequency spectrum of a femtosecond pulse with a center wavelength close to that of the monochromatic source used in the recording process. The diffracted temporal frequency spectrum is modulated by the spatial frequency spectrum of the hologram. Upon transmission through the second lens and the output grating, the diffracted temporal frequency spectrum results in a sequence of short pulses which exhibit one-to-one correspondence with the 1-D spatial distribution in the input image. The resultant sequence of temporal pulses is carried by a single beam of the same spatial frequency.

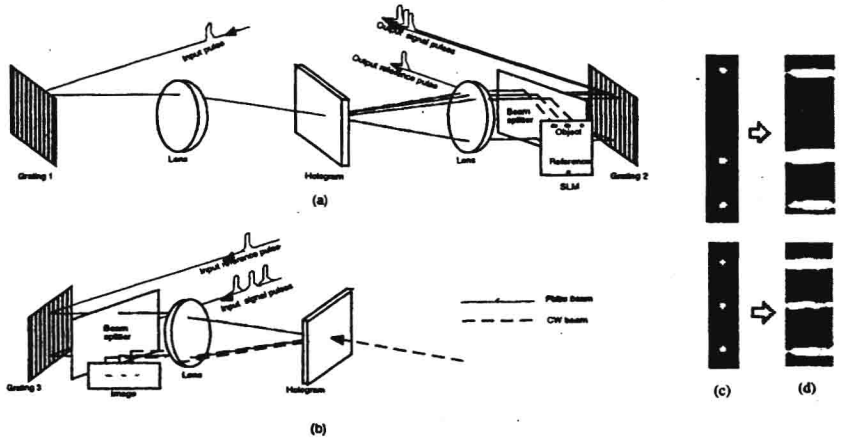

Fig. 1 Schematic diagram of optical processors for (a) parallel-to-serial conversion and (b) serial-to-parallel conversion, and experimental result of image transmission using parallel-to-serial and serial-to-parallel conversion: (c) the original 1-D image, (d) the received 1-D image

At the receiver node we perform an inverse serial-to-parallel transformation. Such a transformation can be realized with spectral holography of the sequence of temporal pulses and a reference pulse as shown schematically in Fig. 1b.[8,9] In the experiments we used 150 fs optical pulses at a wavelength of 480nm. During these experiments the output pulses from the system shown in Fig. 1a were transmitted directly to the input of the system shown in Fig. 1b. Two 1-D binary input images (see Fig. 1c) were used in our experiments for parallel-to-serial and serial-to-parallel conversion employing the processors shown in Fig. 1a and 1b, respectively. The transmitted 1-D image in Fig. 1d shows exact correspondence to the original image in Fig. 1a.

Photorefractive materials provide the high resolution and wide dynamic range necessary for recording and reconstruction of the spectral filters. In addition, with our approach the input signals are Fourier transformed optically into the spectral domain, thus alleviating the need for time-consuming electronic Fourier transform calculations used in the pulse shaper with programmable masks. The speed of this parallel-to-serial conversion is limited by the time response of the bulk photorefractive material, which, depending on the material, can vary in the range of seconds to microseconds.

2.1.3 Cascaded Second-order nonlinearity (CSN)

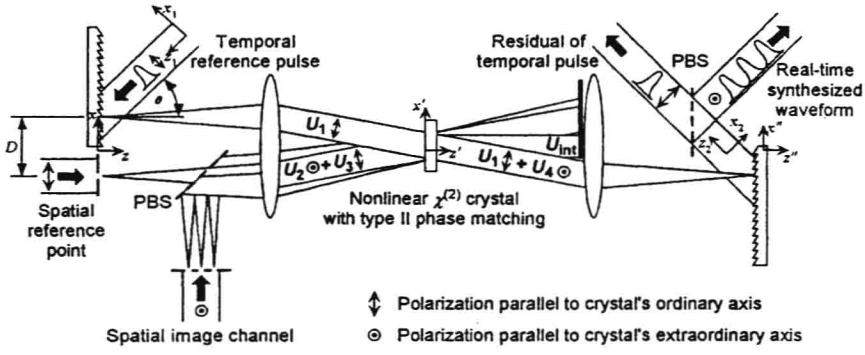

Fig. 2 Experimental setup of the spatial-temporal converter. The CSN enables time-space information exchange via a four-wave mixing process.

The first successful realization of a real-time space-to-time conversion technique capable of generating synthesized temporal waveforms at the output, controlled by a spatial domain image with a femtosecond response time and high conversion efficiency[10]. The nonlinear process, based on a cascaded second-order nonlinearity (CSN)[11,12] arrangement, consists of a frequency-up process followed by a frequency-down process satisfying the type-II non-collinear phase matching condition. The non-linear wave mixing in our experiment takes place in the Fourier domain of the temporal and spatial channels (see Fig. 2). The first nonlinear process of the cascade mixes the Spectral Decomposition Wave (SDW) field U_1 of an ultrashort input pulse, with the spatial Fourier Transform (FT) field U_2 of a quasi-monochromatic wave spatially modulated by a one-dimensional image. The fields U_1 and U_2 are polarized in the ordinary and extraordinary direction, respectively, relative to the optical axis of the nonlinear crystal and their propagation directions satisfy the phase matching condition. The waves U_1 and U_2 generate the intermediate up-converted wave $U_{int} \sim \chi^{(2)} U_1 U_2$, oscillating at the sum frequency, propagating along the optical axis of the setup, and polarized in the extraordinary direction. The second nonlinear process of the cascade mixes the intermediate wave U_{int} and the spatial FT of a narrow slit (implementing a one-dimensional spatial Dirac δ-function), U_3. The narrow slit in the second spatial channel is illuminated by the same quasi-monochromatic source as U_2, and co-propagates with U_2 after a polarizing beam splitter (see Fig. 2). The wave U_3 is polarized in the ordinary direction and interacts with the extraordinary polarized intermediate wave U_{int}. Since U_3 contains no information in either the space or the time domain, its function is to down-convert the carrier frequency of the complex field of U_{int}. In this arrangement, the phase matching condition for the down-conversion process is automatically satisfied. The resultant wave, $U_4 \sim \chi^{(2)} U_{int} U_3^*$, propagates in the same directions as U_1 and at the same center frequency but in an

orthogonal polarization state. The resultant wave is therefore proportional to the input waves as $U_4 \sim (\chi^{(2)})^2 U_1 U_2 U_3^*$, which is equivalent to a four-wave mixing process. When comparing the expression for the resultant wave to the SDW of the input temporal channel, we can observe that the spatially dispersed frequency components are modulated by the information of the spatial mask. Thus, the femtosecond rate spatial-temporal processing has generated the SDW of the output temporal optical waveform. The SDW U_4 is recombined in the optical setup by a second FT lens and grating diffraction to yield the output temporal signal. This synthesized waveform is a convolution of the input ultrashort pulse with a space domain image, whose spatial dependence has been converted to temporal dependence in the spatial-temporal processor. When the duration of the ultrashort pulse is much shorter than the feature size of the temporally mapped mask, then $p(t)$ can be approximated by a Dirac δ-function and the output temporal waveform is directly proportional to the information in the mask.

We demonstrate experimentally the CSN spatial-temporal wave mixing using ultrashort pulses of 100 fs duration at a center wavelength of 800 nm with an energy level of 1 mJ per pulse (generated from a Ti:Sapphire ultrashort pulse oscillator combined with a regenerative amplifier). Ten percent of the power of the laser pulse is split off and introduced into the temporal input channel of the processor, generating the SDW U_1. The SDW is generated by a 600 lines/mm blazed grating and a lens of 375 mm focal length. The remaining 90% of the pulse power is used to generate the light source for the implementation of the spatial channels by stretching the pulse width with a grating pair to a several picosecond duration (i.e., chirped pulse), matching the time window of the temporal channel. The stretched pulse is divided into the two spatial channels for implementing waves U_2 and U_3. Since the CSN process occurs with femtosecond-scale time response due to the fast nonlinearity, a sufficient condition for the four-wave mixing operation is for the two spatial channels to be instantaneously equal. The spatial-temporal wave mixing by the $\chi^{(2)}$ media is performed in a 2-mm thick type II β-barium borate (BBO) crystal. In our experiment, the entire process is derived from a single pulse from the laser source; thus, the information exchange is done on a single-shot basis. The maximum conversion efficiency of the input SDW U_1 to the filtered output SDW U_4 is 10%, limited by fundamental wave depletion. The high conversion efficiency illustrates the advantage of the CSN approach as opposed to conventional $\chi^{(3)}$ nonlinearity for four-wave mixing.

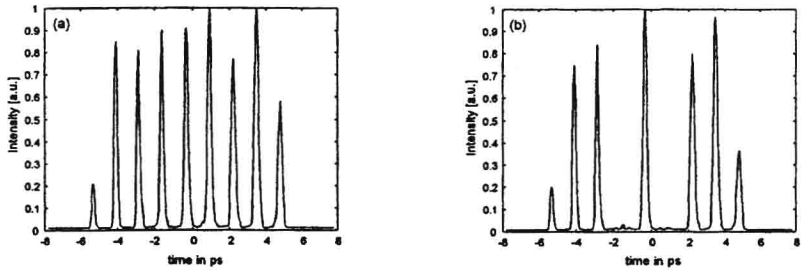

(a) (b)

Fig. 3 Synthesized temporal waveform generated by a spatial information mask consisting of a sequence of equally spaced point sources. (a) All point illuminated by quasi-monochromatic light. (b) Two point sources blocked.

In our first spatial-temporal information transfer experiment, we use a mask containing a sequence of narrow slits spaced 0.8 mm apart. To achieve high light throughput, the illuminating beam is focused into the slits with a cylindrical lenslet array. The shaped waveform, consisting of a sequence of pulses, is observed with a real-time pulse imaging technique (see Fig. 3). As predicted, the synthesized waveform consists of a sequence of pulses separated by ~1.3 ps (mapping spatial separation of 0.8 mm to time). Selectively blocking some of the slits results in a matching temporal waveform, confirming our ability to perform single-shot temporal waveform synthesis in real-time from a spatial channel. These results are generated under maximal conversion efficiency, where fundamental wave depletion is observed. Therefore, by blocking some of the slits, more photons are upconverted by the spatial waves of the open slits, leading to an amplitude distribution change in the pulse sequences of Fig. 2. No evidence of crosstalk between the channels is detected.

Generation of synthesized square pulses by spectral filtering is not a simple task. The mask should contain amplitude information over a wide dynamic range as well as phase information for implementing negative values. Space-to-time mapping techniques simplify the task of complex mask preparation, while the requirement for a wide dynamic range in the recording medium remains. In our wave-mixing approach with CSN, the amplitude of the synthesized wave is dependent upon the amplitudes of the three input waves (as long as wave depletion and phase mismatch are negligible). This linear relationship gives rise to high-fidelity conversion from space-to-time. An adjustable slit is placed in the spatial information channel to experiment with several synthesized square pulse duration. The generated waveforms are modified in real-time by changing the slit width, and the square pulses are immediately observed with the pulse imager on a monitor. At wide slit widths, non-uniformity across the top of the square pulse is observed (see Fig.4). We have verified that the reason is due to non-uniformity in the illumination of the spatial channel. An image of the spatial information channel in the space-to-time processor matches well with the observed image of the synthesized waveform in the time-to-space converter.

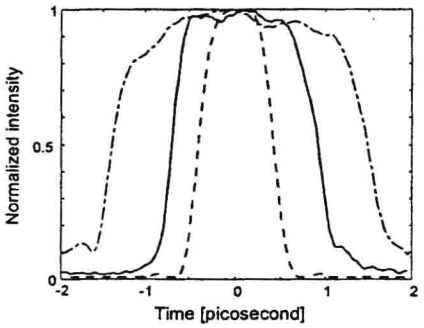

Fig. 4 Superimposed images of square pulses generated by a varying the width of a square aperture in the spatial channel.

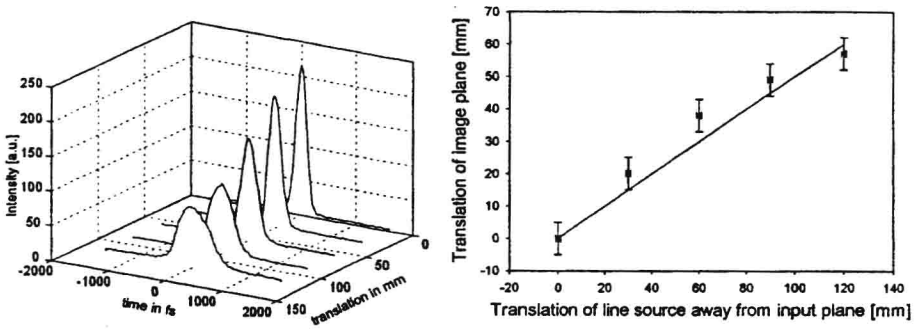

(a) (b)

Fig. 5 (a) Synthesized temporal waveforms generated by a quadratic wave front in the spatial channel, generating chirped pulses. Quadratic wave front generated by longitudinally translating a point source from the input plane. (b) Linear correspondence between translation of point source away from input plane of space-to-time converter and translation of image formation plane in the pulse imager. Solid line corresponds to theoretical curve of slope 1/2.

To demonstrate the ability to encode phase information, a point source, generated by focusing the spatial beam with a cylindrical lens, is used as the spatial information channel. Translating the lens longitudinally away from the input plane forms a spherical wavefront with variable quadratic phase on the input plane of the spatial information channel. As the translation of the line source from the input plane is increased (in either the positive or the negative direction), the output SDW acquires a larger positive or negative quadratic phase and after recomposing on the output grating, emerges as a chirped pulse (either a

positive or negative chirp). The measured synthesized chirped pulses exhibit, as expected, broader pulses along with a reduction of the peak intensity (see Fig. 5a). We estimate the amount of chirp using the pulse imager and as expected we find direct correspondence between the longitudinal translation of the focusing lens and the amount of chirp on the synthesized waveform. We have verified experimentally the relation by finding the location where the output of the pulse imager focuses, for each translated location used in the spatial channel of the space-to-time converter (see Fig. 5b). Thus, we have a correspondence between the longitudinal translation of the line source in the input spatial channel of the spatial-temporal processor and the longitudinal translation of the focus plane of the pulse imager.

Relative to other spatial-temporal processing techniques, the CSN approach provides femtosecond rate processing due to the fast bound electron nonlinearity and high efficiency on account of a relatively large $\chi^{(2)}$ coefficient. The spatial-temporal process that we have demonstrated generates an output temporal waveform that can be reconfigured in real time and is proportional to the convolution of an input ultrashort pulse and a spatial image. Furthermore, wavelength tuning of the synthesized temporal waveform can be achieved by using different temporal frequencies in the two spatial channels (with a correction to the propagation direction, to satisfy phase matching). For operation with pulsed lasers at high repetition rates, the spatial channels may be implemented by a second intense CW laser source, or, the conversion efficiency of the CSN process should be improved. Since the technique realizes a general four-wave mixing process of temporal and spatial information-carrying waves, the setup may be converted to provide the convolution or correlation signal between spatial and temporal channels, with the output in either the temporal or the spatial domain. Thus, this spatial-temporal process can be considered a fundamental system for performing ultrafast signal processing on optical waveforms in the time and space domain.

2.2 Time-to-space Conversion Processors (TSCP)

The TSC processor performs serial-to-parallel demultiplexing of the shaped pulse train created by the STC processor back into parallel spatial domain for electronic detection. The speed requirement of TSCP is even higher than STCP, since the conversion speed needs to match the bit rate of the temporal signal generated by the PS (in the range of THz). The purpose of the PIC is to "slow down" the pulse signals by converting the signals into parallel channels where each channel possess a reduced bit rate of 10-100 GHz that is within the operational bandwidth of the electronic detectors. Therefore, the concern here is how to achieve an optical serial-to-parallel conversion at such high speed of operation. Since the photorefractive four-wave mixing approach suffers from slow time response and does not meet the speed requirements of the demultiplexer, we have demonstrated an alternative approach based on nonlinear three-wave mixing that overcomes the speed limitations of photorefractives. We have developed two approaches to realizing TSCP: a pulse imager and a single shot correlator.

2.2.1 Femtosecond Pulse Imager[13]

Our first TSCP system[13] is capable of real-time conversion of a femtosecond pulse sequence into its spatial image. The approach employs nonlinear spectral domain 3-wave mixing in a crystal of LiB_3O_5 (LBO), where the spectral decomposition waves (SDW) of a shaped femtosecond pulse are mixed with those of a transform limited pulse to generate a quasimonochromatic second harmonic field. Through this nonlinear process, the temporal frequency content of the shaped pulse is directly encoded onto the spatial frequency content of the second harmonic field, producing a spatial image of the temporal shaped pulse.

The femtosecond laser output is split into two beams, one to be used as a reference beam and the other sent into a pulse shaping device (see Fig. 6a) to create a shaped pulse. The shaped pulse and the reference pulse beams are then introduced into the pulse imaging system of Fig. 6b. The two metallic blazed gratings of 600 lines/mm and the two incident beams are arranged vertically in order to obtain the necessary spectrum inversion of the corresponding SDW. These two beams are then introduced into the LBO nonlinear crystal where under the condition of noncollinear phase matching, the second harmonic field will be generated and propagate in a bisector direction that is parallel to the optical axis of the system. A second lens is used to perform a spatial Fourier transform of the second harmonic quasimonochromatic field, producing an image that is detected by a CCD camera.[13]

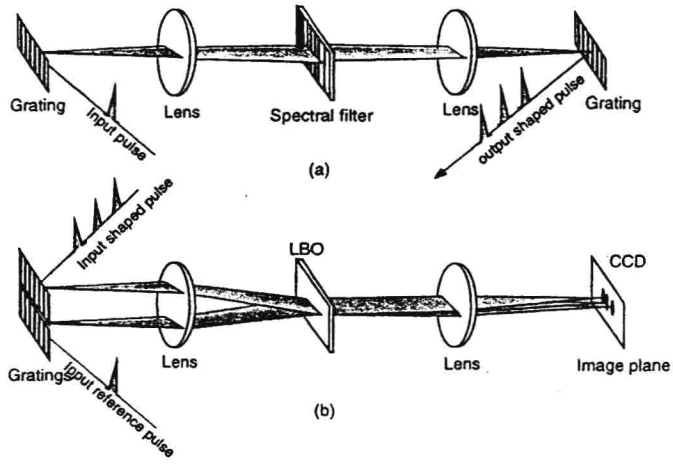

Fig. 6. Schematic diagram of (a) the pulse shaping device with a spectral domain spatial filter and (b) the femtosecond pulse imaging system based on nonlinear spectral domain 3-wave mixing in LBO crystal.

In our experiments, we use a 50/50 binary amplitude grating (i.e., a Ronchi grating) as a spectral filter in the pulse shaping device. Such a grating has a unique property that its Fraunhofer diffraction pattern does not have even diffraction orders except the zero-th order. The pulse image (see Fig. 7) clearly shows that the even order pulses in the sequence (except the 0-th order) do not appear. The three central pulses (i.e., -1, 0, +1 orders) are close together while the other pulses (corresponding to higher orders) are separated by twice the distance. We estimate the distances between the center pulses to be 1.75 picoseconds which is consistent with the theoretical prediction.

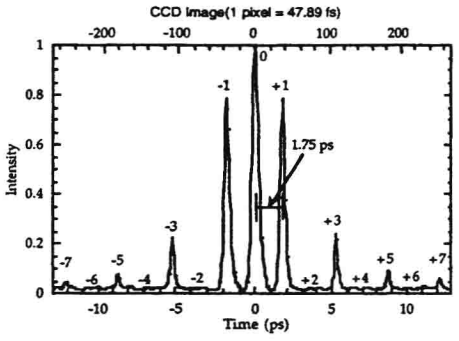

Fig. 7 The images of shaped pulses obtained with femtosecond pulse imaging system of The shaped pulses are obtain using a pulse shaping device with spectral filter implemented by a Ronchi grating.

2.2.2 Femtosecond Single Shot Correlation System: A Time Domain Approach[14]

Our second TSCP technique[14] uses a grating at the entrance of the system, introducing a Transverse-Time-Delay (TTD) into the transform limited reference pulse. The shaped signal pulse and the TTD reference pulse are mixed in a nonlinear optical crystal producing a second harmonic field that carries the spatial image of the temporal shaped signal pulse. The time scaling of the system is set by the magnification of the anamorphic imaging system as well as the grating frequency and the time window of the system is set by the size of the grating aperture. Our experimental results show a time window of 20 ps.

The new pulse correlation technique is shown schematically in Fig. 8. It employs a grating at the entrance of the anamorphic imaging system, introducing a tilt in the pulse front with respect to the wave front. This tilt of the pulse front causes a Transverse Time Delay (TTD) across the spatial extent of the pulse. Next, the shaped signal pulse and the TTD reference pulse are mixed in a nonlinear optical crystal at the image plane of the anamorphic imaging system, producing a second harmonic field. Our technique allows for decoupling of the time delay from the propagation direction, permitting us to select the angle between the intersecting pulses in the vertical direction (see angle ϕ in Fig. 8) to achieve the phase matching conditions for the best efficiency. The time scaling of the system is set independently by adjusting the pulse front tilt angle θ in the orthogonal, horizontal direction.

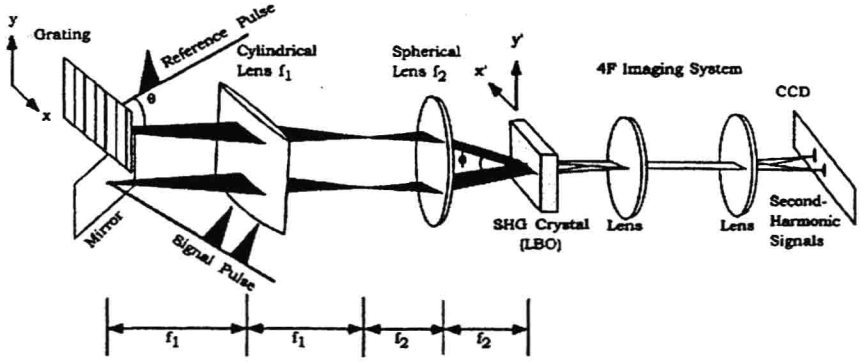

Fig. 8 Schematic diagram of the experimental TTD time domain pulse correlation system: the tilted time front is in the x-direction, enabling the use of the y-direction for optimizing the phase matching conditions of the SHG process

The experimental setup is schematically shown in Fig. 8. We use a mode-locked Ti:Sapphire laser producing 200fs pulses with center wavelength of λ= 920 nm. The laser output beam is collimated and magnified before entering the pulse correlation system to ensure that the spatial intensity profile of the pulse is uniform across the crystal aperture. The optical pulse entering into the pulse correlation system is split into two beams by a beam splitter; one beam is used to provide a reference pulse and the other a signal pulse. The latter can be introduced into a pulse-shaping device to generate a pulse sequence employing spectral domain filtering of the initial pulse.

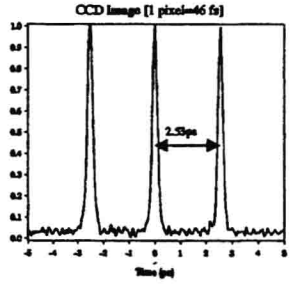

Fig.9 Shaped pulses obtained with the TTD pulse correlation system obtained using a pulse shaper with a phase spectral filter having 3 diffraction orders of equal amplitude

The reference pulse impinges on a metallic blazed grating of 600 lines/mm. The anamorphic imaging system consists of a cylindrical lens and a spherical lens. The two beams are imaged in the horizontal direction, x, and focused in the vertical direction, y, at the back focal plane of the second lens. The signal and the reference beams are parallel to each other with a vertical separation to introduce an angle of the intersection of two pulse beams in the focal plane of the second lens. This angle is optimized to satisfy the phase matching condition in the SHG crystal. A delay line is inserted in the path of the signal beam to control the overlap between the signal and reference pulses in time and space in the volume of the

nonlinear optical crystal. A nonlinear optical crystal LiB_3O_5 is placed in the image plane of the system. The crystal cut and the crystal orientation are designed to satisfy the type I phase-matching condition for non-collinear second-harmonic generation. With this setup, the generated second-harmonic field propagates in the vertical bisector direction, coinciding with the direction of the optical axis of the system. Background noise is spatially filtered, and a dichroic filter is placed in front of the CCD camera to block IR pulses.

We perform pulse imaging experiments with shaped pulses obtained at the output of the pulse-shaping device. We prepare a sequence of pulses using this filter in the pulse shaper and then use our pulse correlation system to analyze this signal. The experimental results are shown in Fig. 9. The three pulses separated by 2.53 ps show excellent agreement with the calculated separation value of 2.50 ps.

3. TEMPORAL INFORMATION PROCESSING

3.1. Time Domain Imaging and information processing

In order to perform time-domain imaging, a time lens is necessary. Kolner and Nazarathy[15] first proposed the concept of the time lens by using the self-phase modulation of an optical short pulse propagating in a piece of fiber to generate additional frequencies and then subsequently compressing the pulse by a pair of gratings as an example of time-domain imaging. The example shows a very important element that is required to perform time-domain imaging. Similar to spatial domain imaging that expands or compresses the spatial frequency bandwidth of the spatial image from the object plane onto the image plane, temporal imaging requires us to vary the spectral bandwidth of the temporally distributed optical signal. However, unlike in spatial imaging, such temporal spectral expansion or compression is a nonlinear process. Thus, the implementation of time-domain imaging requires nonlinear optical processors. Later, Bennett and Kolner[16] demonstrated the time-domain imaging by using a nonlinear up-conversion process. In their experiment, they were able to "slow down" a sequence of 100Gb/sec pulse train into 8.55 Gb/sec.

With the availability of time-lenses, traditional spatial optical information processing techniques can be directly borrowed from and applied to time-domain optical information processing, such as in Fourier filtering[17] and holography [7, 18,19]. Here we present a nonlinear processor that allows one to perform time-reversal of temporal optical signals.

3.2 Instantaneous Time-Reversal and Phase-Conjugation of Ultrafast Waveforms[20]

We report the generation of a true time-reversed waveform for complex amplitude ultrafast waveforms, by inverting the spectral information of the signal about the center frequency. We perform the two time reversal techniques—conventional spectral phase conjugation and the novel spectral information inversion—by wave mixing four spectrally decomposed waves utilizing a cascaded process in a $\chi^{(2)}$ nonlinear crystal. The unique attributes of our approach include instantaneous (femtosecond-scale) response time, high conversion efficiency and a long time-window.

In contrast to the previously demonstrated spatial-temporal processor, the arrangement in this experiment consists of wave-mixing spectrally decomposed waves (SDW). We introduce three ultrafast waveforms to the spectral processing device (SPD): a complex amplitude temporal information waveform and two transform-limited ultrashort pulses, to serve as reference pulses (see Fig. 10). In the spectral inversion arrangement case, the spectral decompositions of the ultrafast waveforms are spatially dispersed in opposite directions by diffracting from a grating +1 and -1 orders at the SPD's input.

The spectrum of the wave U_2 is inverted with respect to the spectra of U_1 and U_3 due to the opposite directions of spatial dispersion corresponding to the +1 and −1 diffraction orders. The frequency-sum process mixes the SDW U_1 and U_2, generating the intermediate wave $U_{int}=\chi^{(2)}U_1U_2$. Due to the energy conservation principle, the intermediate wave is quasi-monochromatic at every spatial location x'. The spectral information from the input temporal signal is preserved in the wave mixing process, and is converted to spatial modulation of the intermediate wave. These two desirable properties were used in the past to perform ultrafast waveform imaging. The second nonlinearity in the cascade is a frequency-difference process that mixes U_{int} with the SDW of U_3, generating an output SDW $U_4=\chi^{(2)}U_{int}U_3^*$. The spectral information in $S(\bullet)$ is inverted with respect to the spatial dispersion direction, thus achieving our goal of spectral information inversion. The SDW U_4 is recomposed by the second grating of the SPD to yield the output temporal waveform $y(t) = s(-t) \otimes r(t) \otimes r^*(t)$, where $\otimes$ denotes the convolution operator.

As $r(t)$ is a transform limited reference pulse, the conjugation term on the last expression may be dropped. The generated output signal is therefore proportional to the time-reversed signal waveform convolved twice with a reference pulse, broadening the temporal features of the signal waveform. The processor's time window can be tailored to the desired application, usually in the several picosecond range.

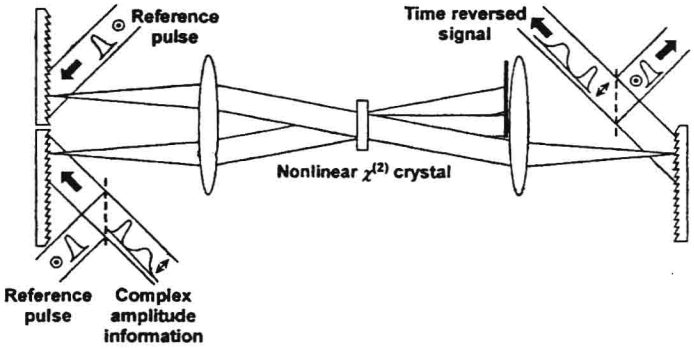

Fig. 10 Experimental setup for true time reversal: Nonlinear four wave mixing of mutually inverted spectrally decomposed waves by CSN results in instantaneous time reversal of complex amplitude ultrafast waveforms.

Our second time reversal experiment is based on generating the phase conjugate of the signal spectrum, useful for time reversal of real amplitude waveforms as well as dispersion compensation in transmission links. The arrangement of Fig. 10 is modified such that the three waves enter the SPD from the same direction, utilizing the same diffraction order, and the signal information wave is used to instigate the down-conversion process. We find that the output temporal waveform in this case is $\hat{y}(t) = s^*(-t) \otimes r(t) \otimes r(t)$. The only difference in the two resulting time reversed waveforms, $\hat{y}(t)$ and $y(t)$, is the conjugation operation on the signal waveform. If one constrains the information signals to contain only real data, the time reversal and the phase-conjugate results are equivalent. For complex amplitude information, the two results will differ.

Both time reversal experiments were performed in a SPD consisting of 600 line/mm blazed gratings and lenses of 375 mm focal length, with a 2-mm long β–barium borate (BBO) crystal placed in the Fourier plane. The three input waveforms were derived from a single ultrashort pulse (generated from a Ti:sapphire ultrashort pulse oscillator combined with a regenerative amplifier) with 100 fsec duration, center wavelength of 800 nm, and energy level <1 mJ. The signal waveform contained 10% of the optical power and the remaining 90% were used for the reference pulses (which serve as pump waves), to maximize the conversion efficiency. To demonstrate the true time reversal property of complex amplitude waveforms by wave mixing oppositely dispersed SDW's, we used a complex waveform signal consisting of a transform limited pulse followed by a positively chirped pulse. The waveform was generated by an unequal arm Mach-Zender interferometer with a grating pair placed in one arm. The input information signal, $s(t)$, and the two time-reversed waveforms, $y(t)$ and $\hat{y}(t)$, were analyzed by a real-time ultrafast waveform imaging system, which has the following desirable property: the quadratic phase—mapped onto the spatial domain—is compensated by free space propagation, i.e., by displacing the output detection plane of the imager. In this manner, the magnitude and sign of the quadratic phase term of the ultrafast waveform that is imaged can be measured.

Figure 11 shows the experimental results of ultrafast waveform imaging for the input information signal, $s(t)$, and the two time-reversed waveforms, $y(t)$ and $\hat{y}(t)$, illustrating the difference between the two techniques of generating time reversed waveforms. The input temporal signal consists of a transform limited pulse followed by the chirped pulse (see Fig. 11-(a)). By displacing the observation plane closer to the Fourier transform lens, the quadratic phase is canceled and the chirped pulse is focused to its tightest spot (see Fig. 11-(d)). Both time reversal methods exchanged the location of the two pulses (see Figs. 11 (b)-(c)). The true time reversal experiment preserved the quadratic phase sign information, as evident by the chirped pulse focusing closer to the lens (see Fig. 11-(e)), whereas the phase conjugate signal reversed